Electronic Supplement 10

Image sharpening and density slicing: An example using an AVHRR image

Given here are the data, and data processing steps, that led to the density sliced, and sharpened, spectral radiance maps given as Figure 6.6 of Chapter 6. The example uses a TIR (AVHRR channel 4, 10.3–11.3 μm) image of Krafla (Iceland). The image was acquired at 04:47Z on 5 September 1984, by the AVHRR flown on NOAA-7. Krafla's September 1984 eruption had begun shortly before the satellite overpass at 23:49Z on 4 September, so that the image was acquired five hours after eruptive activity began. By 00:30Z on 5 September lava fountains were active along a 8.5 km-long set of en-echelon fissures from which lava sheets, with incipient channels, spread in all directions. At the peak of activity fountains were 20 to 50 m high, with the location and trend of the fissures being mapped in Figure 6.6 of Chapter 6. Lava eventually extended up to 7 km to the north, and built a 24 km^2 lava flow field around the fissure system. While the image, and sensor response to the volcanic hot spot, is described in Electronic Supplement 1, AVHRR-based tracking of the eruption, including a complete time series of hot spot maps and review of detection issues in the NIR, MIR and TIR, are given in Harris *et al.* (1995).

Image sharpening and density slicing

The eruption resulted in a 12 × 5 pixel hot spot in the AVHRR channel 4 image, comprising 47 pixels in the TIR. The heat source was so intense that the MIR was badly smeared and saturated, and largely unusable (see Electronic Supplement 1). Even in the TIR, at the core of the thermal anomaly, 18 pixels had DNs that were less than or equal to the non-zero saturation level defined for AVHRR band 4 on NOAA-7, this being a value of eight (see Electronic Supplement 1 for definition of non-zero saturation). We here use the TIR image to execute the seven processing steps that allow extraction of a sharpened image, the density-sliced version of which serves as a radiant intensity map for the hot spot. To produce this map we use the uncalibrated DN image. Results would be the same if we used a calibrated radiance or brightness temperature image. Use of the DN image saves processing steps and time.

Step 1: Sub-image extraction (Figure S10.1)

To further save on processing time, an 11 × 17 pixel sub-image, centered on Krafla and its hot spot, was extracted from the whole 2048 × 2048 pixel image. Values given in the sub-image of Figure S10.1 are DNs. Following Electronic Supplement 2, DN can be converted to radiance (R*) following the linear conversion

$$R^* = a\,DN + b.$$

The calibration coefficients for this image being a = –0.6161 and b = 152.45. Following Singh (1984), these can be converted to brightness temperature (T*) following,

$$T^* = B \,/\, [1n(R^*) \;-\; A]$$

Where, for channel 4 of the AVHRR flown on NOAA-7, A = 9.2058 and B = –1344.832 (see Electronic Supplement 4). Finally, a non-linear correction needs to be applied to give true brightness temperature (see Electronic Supplement 2), which for the TIR channels flown on NOAA-6 and -7 had the form,

$$T^{n1} \;=\; a_0 \;+\; a_1 T \times a_2$$

For channel 4 of the AVHRR flown on NOAA-7, a_0 = –12.92, a_1 = 1.045 and a_2 = 1 (Singh, 1984). Thus the lowest DN of 5 witnessed in the sub-image relates to a radiance of

$$R^* = (-0.6161)\,(5) + (152.45) = 149.36 \text{ milliwatts}/\text{m}^2\text{-steradian-cm}^{-1}$$

Which converts to a brightness temperature of

$$T^* = (-1344.832) \,/\, [1n(149.36 \text{ mW}/\text{m}^2\text{-sr-cm}^{-1}) \;-\; 9.2058] \;= 320.2 \text{ K}$$

Which, when corrected for non-linearity, gives

$$T^{n1} \;=\; (-12.92) \;+\; (320.2 \text{ K})\,(1.045) \;=\; 321.7\text{K} = 48.6\ ^\circ\text{C}.$$

This is set against a background in which DNs are as low as 137, giving T^{nl} of –4.4°C across the snow covered surfaces surrounding the eruption site.

Finally, given that we have a sub-image centered at a point 143 pixels from nadir, we are viewing the surface at a scan angle (α) of:

$$\alpha = 143 \text{ pixels} \;\times\; 0.95 \text{ mrad per pixel} = 0.136 \text{ rad} = \; 7.8^\circ$$

Following the pixel dimension calculation procedure given in Section 3.3 of Chapter 3, using the detector instantaneous field of view (IFOV, β) for channel 4 of the AVHRR flown on NOAA-7 (1.423 mrad, see Table 3.6 of Chapter 3), we have pixel dimensions of 1.24 × 1.22 km.

Step 2: Threshold application (Figure S10.2)

Next I apply a simple fixed threshold to isolate thermally anomalous, or hot spot, pixels containing active lava and fire fountains. I use, for this image, a DN threshold of 121. All values less than or equal to this value are counted as hot spot pixels. This threshold

	X	138	139	140	141	142	143	144	145	146	147	148
Y												
184		129	129	129	129	131	132	131	131	131	128	128
185		130	129	129	127	129	131	130	129	129	127	127
186		130	129	129	127	127	129	125	126	128	127	127
187		131	130	130	127	126	122	63	84	128	129	126
188		132	130	129	126	124	106	6	4	117	130	125
189		133	131	128	123	118	74	8	7	114	128	124
190		134	132	128	122	115	23	8	8	98	128	123
191		134	133	129	123	118	31	8	5	119	125	124
192		134	132	128	122	106	7	8	53	125	123	126
193		134	131	126	121	65	8	8	80	128	123	127
194		135	131	128	122	78	8	8	83	128	123	127
195		135	131	129	124	114	6	8	56	128	123	125
196		134	131	128	126	121	18	8	45	127	124	125
197		134	131	128	127	124	65	5	101	127	125	127
198		136	132	129	128	127	119	110	123	127	127	129
199		137	133	130	129	128	126	126	127	128	128	130
200		137	135	133	132	129	127	127	129	130	129	131

Figure S10.1 Pixel Digital Number (DN) grid for Krafla sub-image. Image: NOAA-7 AVHRR channel 4 acquired on 5 September 1984 at 04:47Z, received at University of Dundee (Scotland, UK). X,Y rows give pixel position in terms of number of pixels from nadir. Scan increment angle is 0.95 mrad, so scan angle to each pixel can be obtained by multiplying pixel number (in the X-direction) by scan increment angle.
Note: All values given here have been compressed (from the full 0 to 1024 range used by AVHRR) onto the smaller 0 to 255 DN range.

	X	138	139	140	141	142	143	144	145	146	147	148
Y												
184		129	129	129	129	131	132	131	131	131	128	128
185		130	129	129	127	129	131	130	129	129	127	127
186		130	129	129	127	127	129	125	126	128	127	127
187		131	130	130	127	126	122	63	84	128	129	126
188		132	130	129	126	124	106	6	4	117	130	125
189		133	131	128	123	118	74	8	7	114	128	124
190		134	132	128	122	115	23	8	8	98	128	123
191		134	133	129	123	118	31	8	5	119	125	124
192		134	132	128	122	106	7	8	53	125	123	126
193		134	131	126	121	65	8	8	80	128	123	127
194		135	131	128	122	78	8	8	83	128	123	127
195		135	131	129	124	114	6	8	56	128	123	125
196		134	131	128	126	121	18	8	45	127	124	125
197		134	131	128	127	124	65	5	101	127	125	127
198		136	132	129	128	127	119	110	123	127	127	129
199		137	133	130	129	128	126	126	127	128	128	130
200		137	135	133	132	129	127	127	129	130	129	131

Figure S10.2 AVHRR channel 4 DN grid for Krafla on 5 September 1984 at 04:47Z with hot spot threshold applied. Pixels with DN less than or equal to the threshold are contained within the black outline.

isolates 47 hot spot pixels, and delimits the hot spot area marked by the solid black line in Figure S10.2.

Step 3: Density slicing (Figure S10.3)

Density slicing is a method by which the number of gray levels in an image is reduced by redistributing the levels into a smaller number of specified groups. The range of gray levels

included in each group defines a "slice" (Mather, 1987; Cracknell and Hayes, 1991). The total number of gray levels in an image can be 256 (for 8-bit TM-class data) or 1024 (for 10-bit AVHRR-class data), which may be reduced to four or five groups or slices. Each slice is then assigned a color. The slice color should be designed to give the viewer an "intuitive feel for the meaning of the color" in terms of a physical quantity (Mather, 1987, p. 187), in the case of heat flux or temperature white and yellow may indicate the hottest slices, blue the coldest. Such image processing facilitates, or enhances, our ability to define and distinguish features within an image, and allows better visualization of differences across a selected feature.

In our case, we want to better visualize the radiant intensity levels within the hot spot, which has DNs in the range of 0 to 121. We find that ~50 % of the information is conveyed by DNs of less than 60, i.e., 23 of the 47 hot spot pixels have DN < 60. We thus define a telescoped four-slice scheme as follows:

1. Slice 0 applies to all pixels beyond the hot spot,
   i.e., pixels with DN greater than 121, so that slice 0 spans the 122 to 1024 DN range.
2. Slice 1 is obtained by slicing the DN range within the hot spot in half,
   i.e., the slice lower limit = 121 / 2 = 61, so that slice 1 spans the 60 to 121 DN range.
3. Slice 2 is obtained by dividing the 0 to 60 range by 2.5,
   i.e., the slice lower limit = 60 / 2.5 = 24 so that slice 2 spans the 24 to 59 DN range.
4. The remaining values are split equally between the remaining two slices,
   i.e., slice 3 = 12 values spanning the 12 to 23 DN range, and
   slice 4 = 12 values spanning the 0 to 11 DN range.

The DN ranges that define each slice, and colors assigned to each slice, are summarized in Table S10.1, with the density-sliced image being given in Figure S10.3. The aim is to assign hotter pixels hotter colors, thereby moving towards a visually effective hot spot map that slices the hot spot into four levels of radiant intensity or heat flux.

Table S10.1. *Slices applied to density slice the sub-image (see Figure S10.3 and S10.7), along with the colors assigned to each slice and associated heat flux and features.*

Slice	DN Range	Bin size	Slice Color	Heat Flux	Associated Feature
0	>121*	902	Grey	Background	Snow-covered ground free of active lava
1	60–121	62	Red	Low	Mixed lava-free and lava pixels, lava flow fronts
2	24–59	36	Orange	Low-moderate	Active lava
3	12–23	12	Yellow	Moderate-high	Active lava
4	0–11	12	White	High	Lava fountains and active lava

* 122–1024

	X	138	139	140	141	142	143	144	145	146	147	148
Y												
184		129	129	129	129	131	132	131	131	131	128	128
185		130	129	129	127	129	131	130	129	129	127	127
186		130	129	129	127	127	129	125	126	128	127	127
187		131	130	130	127	126	122	63	84	128	129	126
188		132	130	129	126	124	106	6	4	117	130	125
189		133	131	128	123	118	74	8	7	114	128	124
190		134	132	128	122	115	23	8	8	98	128	123
191		134	133	129	123	118	31	8	5	119	125	124
192		134	132	128	122	106	7	8	53	125	123	126
193		134	131	126	121	65	8	8	80	128	123	127
194		135	131	128	122	78	8	8	83	128	123	127
195		135	131	129	124	114	6	8	56	128	123	125
196		134	131	128	126	121	18	8	45	127	124	125
197		134	131	128	127	124	65	5	101	127	125	127
198		136	132	129	128	127	119	110	123	127	127	129
199		137	133	130	129	128	126	126	127	128	128	130
200		137	135	133	132	129	127	127	129	130	129	131

Figure S10.3 AVHRR channel 4 DN grid for Krafla on 5 September 1984 at 04:47Z with density slice applied (see Table S10.1 for density slice key).

Step 4: Pixel sub-sampling (Figure S10.4)

The area of the thermal anomaly defined by the threshold applied in Step 2, plus a one-pixel-wide zone surrounding the anomaly, was extracted – these being the pixels defined using red numbers in Figure S10.4. Each pixel was then divided into a grid of nine equal sized sub-pixels. Given the 1.24 × 1.22 km dimension of the master pixels, each sub-pixel is equivalent to a 413 × 407 m surface area.

	X	138	139	140	141	142	143	144	145	146	147	148
Y												
184		129	129	129	129	131	132	131	131	131	128	128
185		130	129	129	127	129	131	130	129	129	127	127
186		130	129	129	127	127	129	125	126	128	127	127
187		131	130	130	127	126	122	63	84	128	129	126
188		132	130	129	126	124	106	6	4	117	130	125
189		133	131	128	123	118	74	8	7	114	128	124
190		134	132	128	122	115	23	8	8	98	128	123
191		134	133	129	123	118	31	8	5	119	125	124
192		134	132	128	122	106	7	8	53	125	123	126
193		134	131	126	121	65	8	8	80	128	123	127
194		135	131	128	122	78	8	8	83	128	123	127
195		135	131	129	124	114	6	8	56	128	123	125
196		134	131	128	126	121	18	8	45	127	124	125
197		134	131	128	127	124	65	5	101	127	125	127
198		136	132	129	128	127	119	110	123	127	127	129
199		137	133	130	129	128	126	126	127	128	128	130
200		137	135	133	132	129	127	127	129	130	129	131

Figure S10.4 AVHRR channel 4 DN grid for Krafla on 5 September 1984 at 04:47Z with hot spot threshold and pixel sub-sampling scheme. Each parent pixel is split into nine sub-pixels which are delimited by thin black lines. Parent pixel DNs used for image sharpening are highlighted in red.

Step 5: Image sharpening (Figure S10.5)

The image sharpening algorithm of Section 6.1.2.1 of Chapter 6 was applied to produce DNs for each sub-pixel. This involves application of the nine Equations (6.1a) to (6.1i), in the order they are given, to the master pixels and sub-pixels defined in Figure 6.6 of Chapter 6. The results, i.e., the "sharpened" DN values for each sub-pixel, are given in Figure S10.5.

Y \ X	139	140	141	142	143	144	145	146	147	148
185										
186					129 129 129 129 128 127 127 127 128 128 128					
					128 124 123 123 117 119 119 118 124 124 126 128					
					126 122 110 110 99 99 99 106 116 116 125 128					
187				127 126 126 126 122 110 110 99 99 99 106 116 116 125 128 128						
				126 125 123 123 106 92 92 79 71 71 84 103 103 115 128 128						
				126 124 119 119 105 74 74 45 39 39 52 83 83 113 126 126						
188			128 127 126 126 124 119 119 105 74 74 45 39 39 52 83 83 113 126 126							
			127 126 125 125 119 113 113 88 58 58 38 14 14 43 72 66 100 124 124							
			126 124 123 123 117 105 105 83 48 48 17 6 6 19 60 60 103 122 122 127 127							
189			126 124 123 123 117 105 105 83 48 48 17 6 6 19 60 60 103 122 122 127 127							
			125 123 121 121 109 95 95 66 39 39 21 7 7 30 59 59 92 120 120 124 126							
			125 122 119 119 108 82 82 52 28 28 13 8 8 20 57 57 96 117 117 125 126							
190			125 122 119 119 108 82 82 52 28 28 13 8 8 20 57 57 96 117 117 125 126							
			125 122 119 119 100 73 73 47 19 19 14 8 8 29 55 55 89 115 115 122 125							
			125 122 119 119 106 72 72 36 17 17 10 7 7 19 57 57 98 117 117 124 125							
191			125 122 119 119 106 72 72 36 17 17 10 7 7 19 57 57 98 117 117 124 125							
			125 123 119 119 96 71 71 40 17 17 13 9 9 36 64 64 96 121 121 123 124							
			125 122 117 117 101 65 65 29 13 13 12 18 18 38 75 75 110 123 123 124 124							
192		125 125 122 117 117 101 65 65 29 13 13 12 18 18 38 75 75 110 123 123								
		125 125 118 112 112 85 56 56 30 9 9 18 29 29 56 87 87 107 124 124								
		124 124 117 103 103 80 46 46 17 8 8 15 37 37 66 96 96 118 125 125								
193		124 124 117 103 103 80 46 46 17 8 8 15 37 37 66 96 96 118 125								
		124 124 112 96 96 71 40 40 23 8 8 22 42 42 71 102 102 115 125								
		124 124 116 96 96 70 40 40 16 8 8 17 45 45 78 105 105 121 125								
194		124 124 116 96 96 70 40 40 16 8 8 17 45 45 78 105 105 121 125								
		125 125 115 101 101 75 44 44 24 8 8 23 44 44 74 104 104 115 125								
		126 126 120 109 109 88 51 51 18 7 7 15 39 39 69 99 99 120 125								
195		126 120 109 109 88 51 51 18 7 7 15 39 39 69 99 99 120 125								
		126 121 117 117 89 59 59 30 8 8 19 33 33 63 93 93 112 125								
		127 124 121 121 105 65 65 25 10 10 14 29 29 55 89 89 117 125								
196		127 124 121 121 105 65 65 25 10 10 14 29 29 55 89 89 117 125								
		127 125 123 123 100 71 71 42 15 15 23 30 30 59 90 90 111 125								
		127 126 124 124 113 82 82 47 24 24 19 40 40 71 100 100 120 126								
197		124 124 113 82 82 47 24 24 19 40 40 71 100 100 120 126								
		125 125 112 95 95 53 42 42 51 58 58 86 112 112 119 126								
		126 126 121 109 109 92 75 75 69 85 85 107 119 119 125 126								
198		126 121 109 109 92 75 75 69 85 85 107 119 119 125 126								
		127 123 120 120 109 106 106 101 110 110 114 124 124 125 127								
		128 127 125 125 122 120 120 119 121 121 124 126 126 127 127								
199		128 127 125 125 122 120 120 119 121 121 124 126								
		126 126 125 124 124 123 125 125 126 127								
		127 127 126 126 126 126 127 127 128 128								
200										

Figure S10.5 Enlargement of AVHRR channel 4 hot spot at Krafla on 5 September 1984 (04:47Z) with image sharpened DNs.

Step 6: Threshold re-application (Figure S10.6)

The threshold was then reapplied to the sharpened image to plot the sub-pixel location of the anomaly edge.

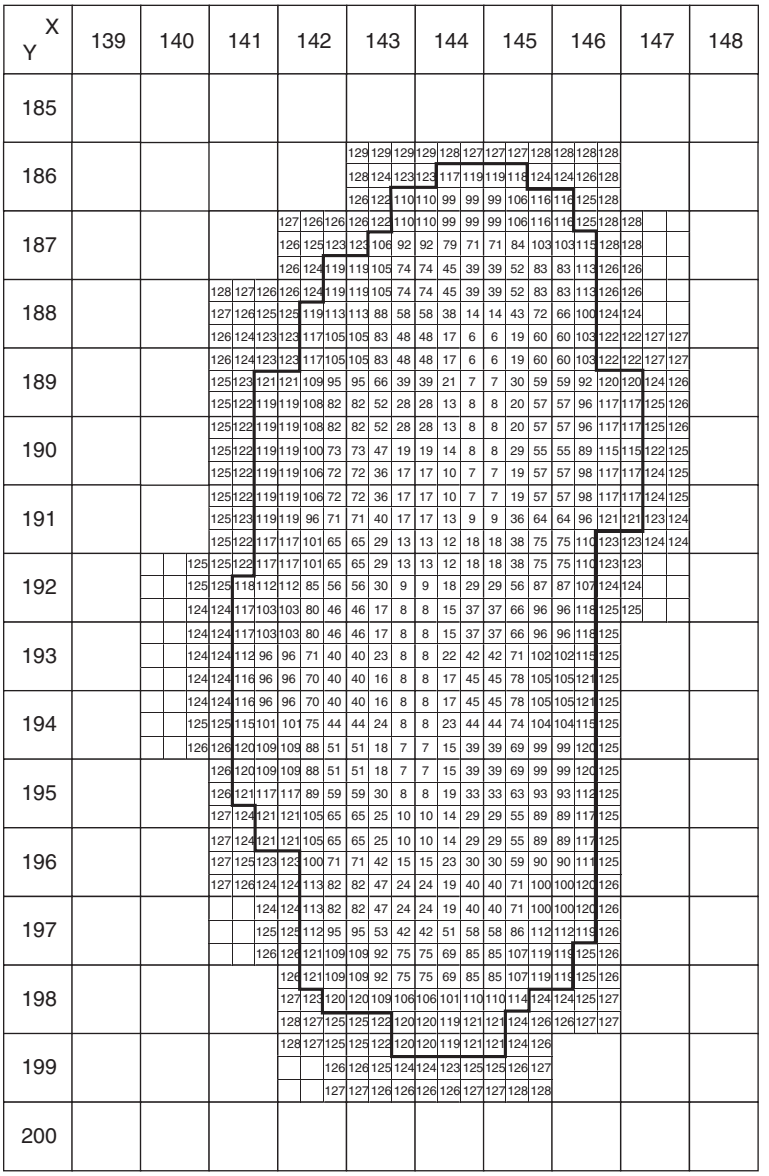

Figure S10.6 Enlargement of AVHRR channel 4 hot spot at Krafla on 5 September 1984 (04:47Z) with sharpened DNs and hot spot threshold applied (thick black line contains hot spot pixels, i.e., pixels with a DN ≤ 121).

Step 7: Density slice the sharpened image (Figure S10.7)

Finally, the sub-pixel DNs of the sharpened image were density sliced using the same bins and colors defined in Step 3 (see Table S10.1).

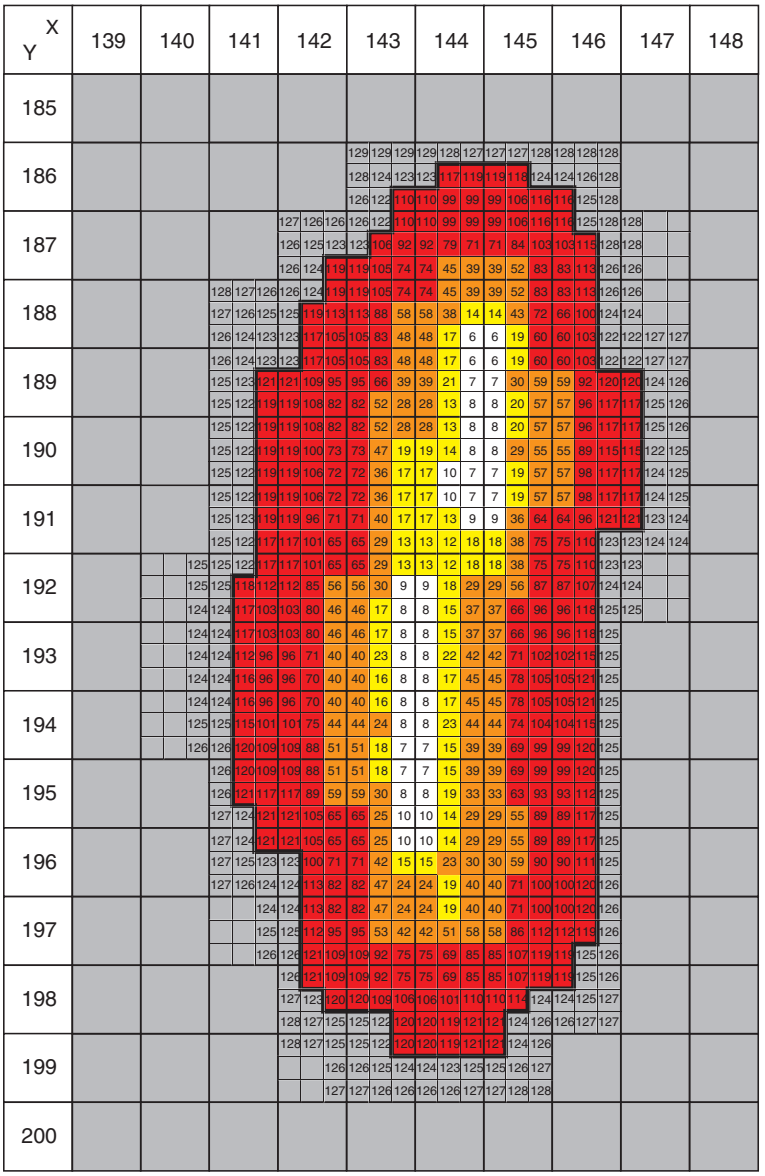

Figure S10.7 Enlargement of AVHRR channel 4 hot spot at Krafla on 5 September 1984 (04:47Z) with image sharpened DNs and density slice applied (see Table S10.1 for density slice key). North is up.

Summation

The density-sliced image and sharpened image, stripped of DNs, is given in Figures 6.6a and 6.6b of Chapter 6. We see that the sharpened image collapses the zone of highest intensity radiances onto the line of active (lava fountaining) fissures, defining a line which is

Figure S10.8 Oblique aerial photograph taken at 00:32 on 5 September 1984, 43 minutes after the September 1984 eruption at Krafla began. The view is due south down the eruptive fissure, of which the entire 8.5 km length is visible. The eruption has reached about maximum intensity, with lava fountaining along each en-echelon fissure segment. Most of the fountains were between 20 and 50 m high (E. Tryggvason, personal communication). Thin, fluid lava is advancing in broad fronts from the entire zone, with darker areas being chilled crust on the active flow surface. (Photo, E. Trggvason).

21 sub-pixels in length, with a slight SSW-NNE trend. Given the ~410 m N-S dimension of each sub-pixel, this is equivalent to a ground distance of 8.6 km, which compares with an observed active fissure length of 8.5 km. An aerial photograph taken 43 minutes after the eruption began, and 4.25 hours before the AVHRR image was acquired, is given in Figure S10.8 for comparison with the density-sliced, sharpened image of Figure S10.7. From the photograph, we see sheets of lava spreading in all directions around the line of fountains, with lava fronts already 1–2 km from the source and the line of fountaining roughly central to the lava flow field. In the density-sliced, sharpened image of Figure S10.7 we see the same pattern, with a high intensity line of radiance centered in the hot spot marking the fountain location, and a lower intensity radiance zone surrounding the central line, these lava pixels extending 7 sub-pixels (or 2870 m) east and west of the central high-intensity line. The feature pattern, geometry and size expressed in the density-sliced, sharpened image of Figure S10.7 thus seems valid, and is an improvement (in terms of level of spatial detail and precision of feature location) over the density sliced radiance map produced from the raw image (see Figure S10.3). It thus appears to be a valid method of producing high spatial resolution radiance maps and feature location estimates from low spatial resolution data.

References

Cracknell, A. P. and Hayes, L. W. B. (1991). *Introduction to Remote Sensing*, London: Taylor & Francis, 293 p.

Harris, A. J. L., Vaughan, R. A. and Rothery, D. A. (1995). Volcano detection and monitoring using AVHRR data: the Krafla eruption, 1984. *International Journal of Remote Sensing*, **16**(6), 1001–1020.

Mather, P. M. (1987). *Computer processing of remotely-sensed images*. Chichester: John Wiley & Sons, 352 p.

Singh, S. M. (1984). Removal of atmospheric effects on a pixel by pixel basis from the thermal infrared data from instruments on satellites. The Advanced Very High Resolution Radiometer (AVHRR). *International Journal of Remote Sensing*, **5**(1), 161–183.

DN grids from:

Harris, A. J. L. (1992). *Volcano detection and monitoring using AVHRR: The Krafla eruption, Iceland, 1984*. Masters Thesis, Department of Applied Physics and Electronics and Manufacturing Engineering, University of Dundee, 206 p.